Icarus 302 (2018) 483–498

Contents lists available at ScienceDirect

Icarus

journal homepage: www.elsevier.com/locate/icarus

Laboratory simulations of planetary surfaces: Understanding regolith physical properties from remote photopolarimetric observations

Robert M. Nelson[a,b,*], Mark D. Boryta[b], Bruce W. Hapke[c], Kenneth S. Manatt[d], Yuriy Shkuratov[e], V. Psarev[e], Kurt Vandervoort[f], Desire Kroner[b,g], Adaze Nebedum[b], Christina L. Vides[b,f], John Quiñones[b,h]

[a] Planetary Science Institute, Pasadena, CA, USA
[b] Mt. San Antonio College, Walnut, CA, USA
[c] University of Pittsburgh, Pittsburgh, PA, USA
[d] Jet Propulsion Laboratory, Pasadena CA, USA
[e] Karazin University, Kharkiv, Ukraine
[f] California Polytechnic State University at Pomona, Pomona, CA, USA
[g] University of California at Los Angeles, Los Angeles, CA, USA
[h] California State University at Los Angeles, Los Angeles, CA, USA

ARTICLE INFO

Article history:
Received 8 September 2017
Revised 15 November 2017
Accepted 20 November 2017
Available online 5 December 2017

Keywords:
Europa
Photometry
Jupiter, satellites
Polarimetry
Satellites, surfaces
Radiative transfer

ABSTRACT

We present reflectance and polarization phase curve measurements of highly reflective planetary regolith analogues having physical characteristics expected on atmosphereless solar system bodies (ASSBs) such as a eucritic asteroids or icy satellites. We used a goniometric photopolarimeter (GPP) of novel design to study thirteen well-sorted particle size fractions of aluminum oxide (Al_2O_3). The sample suite included particle sizes larger than, approximately equal to, and smaller than the wavelength of the incident monochromatic radiation ($\lambda = 635$ nm). The observed phase angle, α, was $0.056^{\circ} < \alpha < 15^{\circ}$. These Al_2O_3 particulate samples have very high normal reflectance ($> \sim 95\%$). The incident radiation has a very high probability of being multiply scattered before being backscattered toward the incident direction or ultimately absorbed. The five smallest particle sizes exhibited extremely high void space ($> \sim 95\%$).

The reflectance phase curves for all particle size fractions show a pronounced non-linear reflectance increase with decreasing phase angle at $\alpha \sim < 3^{\circ}$. Our earlier studies suggest that the cause of this non-linear reflectance increase is constructive interference of counter-propagating waves in the medium by coherent backscattering (CB), a photonic analog of Anderson localization of electrons in solid state media.

The polarization phase curves for particle size fractions with size parameter (particle radius/wavelength) $r/\lambda < \sim 1$, show that the linear polarization rapidly decreases as α increases from 0°; it reaches a minimum near $\alpha = \sim 2^{\circ}$. Longward of ~2°, the negative polarization decreases as phase angle increases, becoming positive between 12° and at least 15°, (probably ~20°) depending on particle size. For size parameters $r/\lambda > \sim 1$ we detect no polarization.

This polarization behavior is distinct from that observed in low albedo solar system objects such as the Moon and asteroids and for absorbing materials in the laboratory. We suggest this behavior arises because photons that are backscattered have a high probability of having interacted with two or more particles, thus giving rise to the CB process.

These results may explain the unusual negative polarization behavior observed near small phase angles reported for several decades on highly reflective ASSBs such as the asteroids 44 Nysa, 64 Angelina and the Galilean satellites Io, Europa and Ganymede. Our results suggest these ASSB regoliths scatter electromagnetic radiation as if they were extremely fine grained with void space $> \sim 95\%$, and grain sizes of the order $< = \lambda$. This portends consequences for efforts to deploy landers on high ASSBs such as Europa. These results are also germane to the field of terrestrial geo-engineering, particularly to suggestions that

* Corresponding author at: Planetary Science Institute, 775 North Mentor Avenue, Pasadena CA 91104, USA.
E-mail addresses: Rmnelson2@earthlink.net, rnelson@psi.edu (R.M. Nelson).

https://doi.org/10.1016/j.icarus.2017.11.021

earth's radiation balance can be modified by injecting Al_2O_3 particulates into the stratosphere thereby offsetting the effect of anthropogenic greenhouse gas emissions.

The GPP used in this study was modified from our previous design so that the sample is presented with light that is alternatingly polarized perpendicular to and parallel to the scattering plane. There are no analyzers before the detector. This optical arrangement, following the Helmholtz Reciprocity Principle (HRP), produces a physically identical result to the traditional laboratory reflectance polarization measurements in which the incident light is unpolarized and the analyzers are placed before the detector. The results are identical in samples measured by both methods. We believe that ours is the first experimental demonstration of the HRP for polarized light, first proposed by Helmholtz in 1856.

1. Introduction

Solar system bodies have been observed for half a millennium at many angular scattering geometries with the telescopic aided human eye, photographic plates and more recently with electronic photonic detectors located on Earth based telescopes, observatories in earth orbit, or on interplanetary spacecraft. Galileo pioneered both astronomical and laboratory reflectance measurements of this type (Galileo, 1616). Since Galileo's work, researchers have undertaken measurements of the reflectance and polarization change of light scattered from solar system bodies with respect to phase angle (α) and compared the results to the reflectance and polarization properties of aerosols and particulates measured in the laboratory in efforts to better understand the ongoing physical processes in clouds, aerosols, planetary ring systems and the textural properties of planetary surfaces. Here, we present laboratory measurements of the photometric properties of materials that simulate high albedo planetary regoliths that are expected on highly reflective atmosphereless solar system bodies (ASSBs).

The increase in reflectance with decreasing phase angle of light scattered from solar system objects, the 'Opposition Effect (OE)' (Gehrels, 1956), has been well documented since the phenomenon was first reported in Saturn's rings (Seeliger, 1895) and the Moon (Barabashev, 1922). The linear polarization change with phase angle, first noted by Umov (1905), has also been well studied in the laboratory for a comparable period (Lyot,1929). Despite extensive scrutiny with earth-based telescopes, telescopes in Earth orbit, remote sensing telescopes in deep space, and laboratory reflectance and polarization phase curve analyses, there is no generally accepted single physical mechanism that explains both the reflectance and polarization phenomenology. Discussion of past astronomical observations and laboratory measurements is found in many locations (Lyot, 1929; Hapke, 1993, 1963, 1966; Dollfus, 1996; Deau et al., 2013; Li et al., 2015; Belskaya et al., 2015; Levasseur-Regourd et al., 2015 and Shkuratov et al., 2015).

Research conducted in recent decades suggests that reflectance and polarization opposition effects can arise from distinct processes depending on the albedo and particle size of the materials being investigated. For low albedo materials, arguments based on geometric optics that involve the shadowing effects of regolith grains upon one another, shadow hiding (SH) have received widespread application in interpreting remote sensing data (Hapke, 1966; Irvine, 1966; Geake et al., 1984). In highly reflective media, constructive interference effects, known in the planetary science community as 'coherent backscattering' (CB), create an OE (Shkuratov, 1985, 1989, 1991, 1992, 1994; Muinonen, 1989).

Our earlier investigations of the change in linear and circular polarization ratio with phase angle have shown that the OE in particulate materials in the form of lunar samples is due to both processes, SH and CB (Hapke et al., 1998). In highly reflective particulate media we have shown that CB is the predominant process. (Nelson et al., 2000, 2002).

SH can be understood in the formalism of geometric optics. It arises because, as phase angle nears zero, shadows cast by one regolith grain upon another become less visible to the remote observer. SH is discussed in Irvine (1966); Hapke (1966, 1981, 1986, 1993) and Lumme and Bowell (1981), Shkuratov et al. (2005), Shkuratov and Grynko (2005), and Stankevich and Shkuratov (2004).

CB can be understood in terms of physical optics processes arising from constructive interference of photons being multiply scattered in the medium. In the physics literature this process is known as 'time-reversal symmetry' and also 'weak photon localization' (Kuga and Ishamaru, 1985; Wolf and Maret, 1985; Akkermanns et al., 1986, van Albada and Lagendijk, 1985, MacKintosh and John, 1988). This work followed from the discussions of the phenomenon known as 'Anderson localization' in solid state media (Anderson, 1958) where electrons propagating through a solid can become temporarily localized and constructively interfere, changing the properties of the solid from a conductor to an insulator. The CB enhancement in multiply scattering media has been compared to an extension of the classical double slit experiment and as being a photonic analogue of the metal-insulator transition seen in Anderson localization (Aegerter and Maret, 2009).

CB arises due to the constructive interference between multiply scattered photons that travel nearly the same path through the material but in opposite directions. As phase angle approaches zero the waves become in phase with each other and constructive interference occurs creating a pronounced OE. As phase angle increases such rays interfere non-coherently and the observed reflectance diminishes rapidly with increasing α. CB has been suggested as the cause of the strong opposition surges of high albedo ASSBs (Shkuratov, 1988; Muinonen, 1990; Hapke, 1990; Hapke and Blewett, 1991; Mishchenko, 1992; Mishchenko et al., 2006).

The CB mechanism posits that the returned radiation is multiply scattered. Experimental and theoretical studies of CB suggest that there should be distinct observational effects if the incident radiation is linearly polarized (Kuga and Ishamaru, 1985) and when the incident light is circularly polarized (Steven and Cwillch, 1986; Etemad et al., 1987). The linear polarization of the scattered light is preserved after a single scattering. However, the helicity of circularly polarized light is reversed at the first scattering. The polarization of the scattered light becomes more randomized as the number of scatterings increases. Since the CB process requires multiply scattered light, the major contribution to a CB induced opposition increase will be due to light that has been scattered twice, and hence the scattered light has the same direction of circular polarization as the light incident on the sample. This has been detected in laboratory GPP experiments by measuring change in the circular polarization ratio (CPR) with respect to phase angle (Nelson et al., 2000, 2002). (CPR is defined as the ratio of light scattered with the same helicity as the incident light to that with the opposite helicity). CPR will increase with decreasing phase angle if CB is the principal process responsible for the scattered light. This increase in the circular polarization ratio is widely regarded

as the characteristic signature of the CBOE because the SH is dominated by singly-scattered light." (Hapke et al., 1993). The SH process does not produce such behavior in the linear and circular polarization ratios. SH effects are expected to be diminished in highly reflective media because multiple scattering of photons between regolith grains would tend to illuminate the shaded areas and randomize the polarization. CB is expected in highly reflective media where multiple scattering of photons between regolith grains occurs. These effects are not restricted to optical wavelengths but are also seen in bi-static radar observations of planetary objects. Combining consideration of the CB and SH effects has been analyzed in Stankevich et al. (2007a, b)

Much of our application of these techniques at optical wavelengths was patterned after techniques pioneered by the radar community (see Patterson et al., 2017).

In our earlier studies (Nelson et al., 2000, 2002) we deconstructed the scattering process using a goniometric photopolarimeter (GPP) which allowed us to measure the reflectance phase curve, the linear and circular polarization ratios, and the linear polarization as a function of phase angle. Our instrument presented samples with light that was linearly polarized in, and perpendicular to, the scattering plane. The reflected light was analyzed in both senses of linear polarization. We also presented the samples with right and left handed circularly polarized light and analyzed it in both senses of circular polarization. We made angular scattering measurements of the light scattered from a simulated planetary surface from 0.05° to 5°. These GPP measurements permitted us to estimate the amount of multiple scattering in a particulate medium in the laboratory. When observing highly reflective materials such as Al_2O_3, the reflectance dramatically increases as phase angle decreases, often by 20–30% between 5° and 0.05° as a consequence of CB of photons that are multiply scattered in the medium. These photometric properties are dependent on the size and the albedo of the regolith particles.

In this work, we:

1. Present new data from our improved instrument.
2. Provide experimental evidence verifying that the Helmholtz Reciprocity Principle (HRP) applies to polarized light as well as scalar.
3. Present a simple expression that closely approximates (for $0° < \alpha < 15°$) the reflectance phase curves measured in the laboratory and also the reflectance phase curves of solar system objects. This enables straightforward comparison between our laboratory data and the phase curves of ASSBs, while (perhaps conveniently) sidestepping competing theoretical constructs.
4. Present a simple expression that closely approximates (when $0° < \alpha < 15°$) the polarization phase curves of well sorted particle size fractions of highly reflective powders (Al_2O_3) and show that they closely approximate the polarization phase curves of ASSBs particularly the three high albedo Galilean satellites Io, Europa and Ganymede.
5. We note the strong resemblance of the polarization phase curves of Europa to those of our samples with porosities exceeding 90%, suggesting that the surface of Europa may have a similar high porosity.

The two empirical expressions approximating the reflectance and polarization behavior are particularly useful to remote sensing observers of small bodies in the outer solar system. These objects are only seen at very small phase angles when observed from Earth or Earth orbit and the telescopic observations at small phase angle may comprise the entire body of information for many ASSBs. Remote sensing observers can easily compare their measurements to laboratory data such as ours and easily assess the photometric properties, and potential hazards to planet Earth, presented by small bodies in the outer solar system that might be deflected inward toward the sun.

2. The observations

We used a GPP to measure the reflectance and polarization phase curves of 13 well-sorted particle size fractions of aluminum oxide (Al_2O_3) industrial optical abrasives with diameters $0.1 \leq d \leq 30\,\mu m$. These samples are identical to those studied in our previous experiments where we measured the reflectance phase curve and addressed the amount of multiple scattering in the materials by measuring the phase angle dependence of the circular polarization ratio (Nelson et al., 2000, 2002; Shkuratov et al., 2002**).**

The Al_2O_3 powders are supplied by the manufacturer in well-sorted size fractions that are larger than, comparable to, and smaller than the wavelength of our incident light ($\lambda = 0.635\,\mu m$). They are chemically stable, permitting repeated investigation over long periods of time by diverse, widely distributed investigation teams. Since our initial investigation, similar angular scattering investigations have been performed on these same Al_2O_3 particulates with GPP instruments at other laboratories around the world, permitting us to understand differences in instrumental performance by comparing identical materials measured on different instruments (Shkuratov et al., 2002; 2006; 2007; Kaasalainen et al., 2002; Piatek et al., 2004; Ovcharenko et al., 2006, Gunderson et al., 2006; Psarev et al., 2017). These particulate materials are excellent planetary regolith analogues for high albedo ASSBs. High albedo ASSBs have been shown to have water ice as a major component (Europa and Enceladus are two clear examples). Al_2O_3 is an excellent analogue due to its hexagonal crystal structure, which matches that of water ice. Crystals of H_2O tend to form platelets that are highly reflective and that tend to align themselves upon settling; this is also true for our powders of Al_2O_3.

The understanding of the photometric properties of Al_2O_3 particulates has assumed increased importance given that proponents of geoengineering have suggested widespread stratospheric distribution of Al_2O_3 as an aerosol a means of terrestrial climate modification (Teller et al., 1997). The highly abrasive nature of Al_2O_3, if distributed on a global scale, has important worldwide health implications for air breathing animals, threatening widespread lung diseases analogous to silicosis – a well know malady that effects the health of quarry workers.

3. Instrument description

The data were taken on the improved 'long arm' GPP, formerly located at Jet Propulsion Laboratory in Pasadena CA and now relocated at the Department of Earth Sciences and Astronomy, Mount San Antonio College, Walnut CA. A GPP instrument of this type is generally classified as a "polarization-sensitive well-collimated radiometer," and the Al_2O_3 samples are classified as "discrete random media" (Mishchenko, 2017).

The particulate samples were illuminated with linearly polarized monochromatic light, alternating back and forth 'in' and 'perpendicular to' the scattering plane. The samples were horizontally and laterally homogeneous. We measured the intensity of the scattered component from $0.05° < \alpha <$ to 15°.

In astronomical observations and in most of the previous laboratory GPP investigations, the incident light is un-polarized; analyzers are placed just before the detector. The sum and cross polarization intensity is measured with respect to the scattering plane - the plane defined by the light source, the sample and the detector. In our new and improved laboratory configuration, polarized light is presented to the sample, and the intensity of the reflected component is measured without an analyzer positioned be-

fore the detector. This reduces the number of optical surfaces that the light must pass and thus improves signal to noise. In addition, the solid-state laser light source controls wavelength exactly and produces a linearly polarized output. The results from either method should be identical following the Helmholtz Reciprocity Principle (HRP) (see Minnaert, 1941, van de Hulst (1957, 1981 chap 5) Chandrasekhar, 1960 p 42, p94, pp171–174) and Hapke, 1963, p 264). For the purpose of this discussion the HRP simply stated is, "In a measurement of the bidirectional reflectance distribution function (reflectance divided by the cosine of the angle of incidence) no difference will result from interchanging the source and the detector."

We first demonstrate that the HRP, advanced by Helmholtz in 1856, applies. We show that these laboratory results, acquired using the HRP design, agree with our previous laboratory investigations of the identical materials which used the traditional methods. In subsequent sections, we discuss the implications of the new set of reflectance and polarization phase curves that we report herewith.

Following discussions advanced in van de Hulst (1957, 1981 chap 5) and Chandrasekhar (1960 p 42, p94, pp171–174), using the formalism of Stokes vectors and Mueller matrices $M_{i,j}$, we may describe the first type measurements as

$$\begin{pmatrix} M_{11}\left(I_\perp + I_\parallel\right)/2 \\ M_{21}\left(I_\perp + I_\parallel\right)/2 \\ 0 \\ 0 \end{pmatrix} = \frac{1}{2}\begin{pmatrix} M_{11} & M_{12} & 0 & 0 \\ M_{21} & M_{22} & 0 & 0 \\ 0 & 0 & M_{33} & M_{34} \\ 0 & 0 & M_{43} & M_{44} \end{pmatrix}\begin{pmatrix} I_\perp + I_\parallel \\ 0 \\ 0 \\ 0 \end{pmatrix}, \tag{1}$$

where $I_\perp + I_\parallel = 2I$, since $I_\perp = I_\parallel$. To characterize the linear polarization producing with this Mueller matrix, it is necessary to divide the resulting second Stokes parameter by the first one, then $P = M_{21}/M_{11}$. The second type of measurements can be present as follows:

$$\begin{pmatrix} (M_{11} + M_{12})I_\perp/2 \\ (M_{21} + M_{22})I_\perp/2 \\ 0 \\ 0 \end{pmatrix} = \frac{1}{2}\begin{pmatrix} M_{11} & M_{12} & 0 & 0 \\ M_{21} & M_{22} & 0 & 0 \\ 0 & 0 & M_{33} & M_{34} \\ 0 & 0 & M_{43} & M_{44} \end{pmatrix}\begin{pmatrix} I_\perp \\ I_\perp \\ 0 \\ 0 \end{pmatrix} \tag{2}$$

and

$$\begin{pmatrix} (M_{11} - M_{12})I_\parallel/2 \\ (M_{21} - M_{22})I_\parallel/2 \\ 0 \\ 0 \end{pmatrix} = \frac{1}{2}\begin{pmatrix} M_{11} & M_{12} & 0 & 0 \\ M_{21} & M_{22} & 0 & 0 \\ 0 & 0 & M_{33} & M_{34} \\ 0 & 0 & M_{43} & M_{44} \end{pmatrix}\begin{pmatrix} I_\parallel \\ -I_\parallel \\ 0 \\ 0 \end{pmatrix} \tag{3}$$

Considering in the experiment described by the Eqs. (2) and (3), $I_\perp = I_\parallel$ we may calculate the polarization degree as follows:

$$P = \frac{(M_{11} + M_{12})I_\perp/2 - (M_{11} - M_{12})I_\parallel/2}{(M_{11} + M_{12})I_\perp/2 + (M_{11} - M_{12})I_\parallel/2} = \frac{M_{12}}{M_{11}} \tag{4}$$

The elements M_{21} and M_{12} related to the first and second type of measurements, respectively, are different generally for an arbitrary geometry of illumination/observation of particulate media. However, in our case, when phase angle is small and samples illuminated along their normal, the elements are very close to each other and essentially equal in these experiments.

For each of the 13 particle size fractions shown in Table 1, the results of many runs were combined and averaged to produce reflectance phase curves and polarization phase curves. These were compared to our previous measurements of the same materials (Nelson et al., 2000, Fig 3; Shkuratov et al., 2002, Fig 14 (lower)). If the HRP applies, then the reflectance and polarization phase curves from this work, based on the HRP, should agree with the 'classical' reflectance and polarization phase curves of the same materials that we reported previously (Nelson et al., 2000,2002; Shkuratov et al., 2002).

The physical properties of the samples, along with the manufacturer's product description are shown in Table 1.

The GPP as initially designed has been described previously (Nelson et al., 2000, p546). The following changes have been implemented since the initial description.

(1) The Helium Neon laser light source ($\lambda = 633$ nm) has been replaced by a solid state laser (Coherent 31-0144-000 LabLaser 635 nm 5 mW C ULN). The output of the solid state laser ($\lambda = 635$ nm) is linearly polarized. For the purpose of comparison with our previous work (Nelson et al., 2000, 2002) this difference in input wavelength (~2 nm) is of no consequence.
(2) A ThorLabs FL05635 FWHM 10 nm blocking filter was located before the detector. This excluded light from the laboratory environment from entering the detector permitting only light of $\lambda = 635$ nm +/−10 nm to enter the detector.
(3) The Hamamatsu R928 photomultiplier tubes, which previously measured the intensity of the scattered light for the signal and reference channels, have been replaced by Hamamatsu C12703 series silicon avalanche photodiode detectors (SAD).
(4) All other filters and analyzers between the sample and the detector have been removed.
(5) The light from the laser that is presented to the sample is alternately polarized parallel to, then perpendicular to, the scattering plane. The linear polarization state of the incident light is changed by inserting half wave plates (Tower Optical A015Z) at appropriate times during data acquisition sequence using a programmed stepper motor.
(6) The arm positioning stepper motor has been replaced by one with a longer screw. This extends the phase angle range to 15°. In our earlier work, this limit was 5°. This is important because the linear portion of the phase curve of most particulate materials may extend beyond 5°. This improved instrument measures the opposition peak and the linear portion of a typical particulate phase curve.

4. Sample preparation

High albedo particulate surfaces have often been simulated in the laboratory using MgO, $BaSO_4$, or powdered, compressed Polytetrafluoroethylene aka Teflon, PFTE, or HALON (Weidner and Hsia, 1981). These materials, while easily available, are not well sorted into particle sizes that are larger than, comparable to, or less than the wavelength of the incident light used in most GPP instruments. Therefore, in 2000, we introduced powdered aluminum oxide, Al_2O_3, as a material appropriate for simulating high albedo regoliths in the laboratory (Nelson et al., 2000). Powdered Al_2O_3 is widely used as an optical abrasive due to its great hardness (Moh's hardness scale #9) and is in great demand by the optics industry. The virtues of mass production permit Al_2O_3 particulates to be acquired at remarkably low cost by laboratory investigators worldwide, allowing experimentalists to compare results from the same materials with the many theoretical models and with spacecraft results as they become widely available. Since our first reports, other extremely reputable laboratories have since reported measurements on these same materials (Shkuratov et al., 2002; 2006; 2007; Kaasalainen et al., 2002; Piatek et al., 2004; Ovcharenko et al., 2006; Gunderson et al., 2006).

Table 1
Physical Properties of the Particulate Materials used in this study.

	Particle size (μm)	Number of runs	void space (%)	Particles per cm^3
GB 3000	0.1	8	97.68	4.43E + 13
GB 2500	0.5	9	96.30	5.66E + 11
GB 2000	1	12	95.50	8.59E + 10
GB 1500	1.2	6	94.94	5.60E + 10
GB 1200	1.5	6	95.81	2.37E + 10
WCA 1	2.1	6	84.60	3.18E + 10
WCA 3	3.2	4	83.10	9.85E + 09
WCA 5	4	4	82.21	5.31E + 09
WCA 9	5.75	4	81.74	1.83E + 09
WCA 12	7.1	8	76.83	1.24E + 09
WCA 20	12.14	8	75.41	2.62E + 08
WCA 30	22.75	6	70.70	4.75E + 07
WCA 40	30.09	6	65.85	2.39E + 07

Al_2O_3 is available from various commercial suppliers in a wide range of particle sizes that are as small as 0.1 μm to several hundred microns. The materials used in this study are supplied by Micro Abrasives Corp of Westfield Mass, USA (http://www.microgrit.com/) and the Stutz Company of Chicago IL, USA (http://products.stutzcompany.com/item/lapping-compounds/aluminum-oxide-optical-finishing-powder/item-1168).

The sample's characteristics are shown in Table 1. The smaller sizes ($d < 1.5$ μm; designated 'GB') have a different morphology from the larger sizes ($2.1 < d < 30.09$ μm; designated 'WCA'). Both the GB and WCA designations were previously offered by Microabrasives Corp. The product identifications and approximate particle sizes are shown in Table 1.

The samples used in this study are identical (i.e. taken from the same packaging lot) to the samples used in our previous investigations. The method of preparation was the same as that described in Nelson et al. (2000, 2002). An identical set of samples from the same manufacturing lot was provided to the Karazin University GPP team and the results were reported by Shkuratov et al. (2002). The same set was also used by Piatek et al. (2004) and Kaasalainen et al. (2002). A typical size distribution about the mean size is shown in Fig. 5 of Nelson et al. (2000). The reflectance ($\lambda = 633$ nm) of each sample measured at a phase angle of 5° relative to HALON is shown in Nelson et al. (2000) Table 1.

The sample cup is 9.2 mm deep and 3.45 cm. in diameter. It is rotated at a frequency of 5–10 rpm in order to average the effect of random interference of photons on multiply scattered paths commonly known as 'laser speckle' . In similar experiments conducted in the physics community this averaging has also been accomplished by measuring the reflectance of small particles in liquid suspension; the Brownian motion of the particles serves the same purpose (van Albada and Lagendijk, 1985; Wolf and Maret, 1985; Aegerter and Marat, 2009).

The size of the laser spot on the sample is ~2.5 mm, far larger than the size of the individual particle sizes under investigation. At any instant, the detector views an average of the light reflected from many individual particles.

For each run the particles were gently poured into the sample cup, the cup was very lightly tapped and tilted until the surface of the particles was level with the rim of the cup. The combined mass of the sample and the cup was measured on a Mettler-Toledo AE200 laboratory balance. We made many runs on each particle size fraction. The average mass in the sample was calculated for each of the 13 particle sizes. We then calculated the number of particles filling the cup, the void space, and the volume density and number density of the particles in each size fraction. The results are shown in Table 1.

We note the high void space (~95%) that is seen in the five smallest particle size fractions. The void space depends on the gravitational force exerted by each layer of particles on the underlying material, and is countered by the van der Waals repulsive forces between each particle. For each particle the mass varies as the volume (r^3) and the van der Waals force varies as the surface area (r^2). We suggest that this porosity increase with decreasing particle size arises as a consequence of the cubic decrease in mass (and downward gravitational force) of each particle as radius decreases being counteracted by the quadratic decrease in surface area with decreasing radius of each particle providing van der Waals repulsion between individual particles. As particle size gets smaller the van der Waals repulsive forces grow larger relative to the downward gravitational forces. This causes the porosity to increase as particle size decreases.

5. The measurements

A Hamamatsu C12703 SAD was located at the end of the GPP movable arm 231 cm. from the surface of the sample cup. A ThorLabs FL05635 FWHM 10 nm blocking filter ($\lambda = 635 + /-10$ nm) was placed before the detector. A second Hamamatsu C12703 SAD observed the reflected light at a constant phase angle throughout the run after it passed through an identical filter.

An individual run consisted of 244 angular scattering measurements as the phase angle was varied from 0.056° to 15° and returned to 0°, 122 measurements were made on the outbound leg and 122 on the inbound leg. The first measurement was made at a phase angle of 0.056°. The GPP movable arm was then was incremented by 0.05° and the next measurement was made. Measurements were made at this incremental rate increase until the phase angle reached 1.2°. The angular position was then incremented in 0.1° steps until the phase angle reached 3°. From 3° to 15° the arm was incremented in 0.15° steps. When the arm reached 15° the process was reversed; the arm position was decremented on the inbound leg in the reverse of the sequence in which it was incremented on the outbound leg.

At each angular positioning, an angular scattering measurement was first made for one polarization state, then the half wave plate at the input laser path was rotated 90°. This changed the polarization of the light presented to the sample by 90° and another measurement was taken. We carefully calibrated the position of the laser and half wave plate such that the polarization was first 'perpendicular to' the scattering plane and then 'in', or 'parallel to', the scattering plane for the second measurement. The polarization of the incident light was alternated four times at each angular position on the outbound and inbound legs of the run and the results were averaged.

At each angular position, the intensity of the reflected signal was recorded 64 times and averaged to comprise an individual data measurement at that position setting. Simultaneously, the reference measurement was compared to the signal as a means of

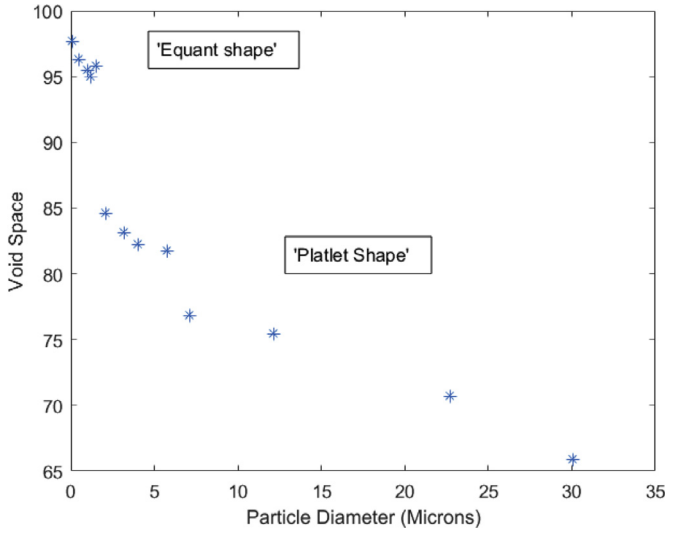

Fig. 1. Particle size vs. void space for 13 Al_2O_3 particulate samples. The platlet shaped particles ($d \geq 2.1\,\mu m$) exhibit greater packing efficiency. The equant particles ($d \leq 1.5\,\mu m$) produce greater void space. These void space results are consistent with those in previous studies (Nelson et al., 2000, 2002).

testing for variations in the output of the laser. We find that the amount of this correction was insignificant.

The incident beam from the laser passed a Stanford Research Systems SRS 540 optical chopper before it was presented to the sample. The chop frequency was ~105 Hz. The output of the signal and reference detectors was analyzed by two Stanford Research Systems SR830DSP Lock-in amplifiers which were tuned to the chopping frequency. The time constant was 300 ms. The signal and reference intensity output of the amplifiers were recorded on a Dell Precision 850 computer. The output arrays were processed on a SONY VAIO VGN-FW486J/H laptop computer and an HP Zbook Mobile Workstation using array processing procedures we developed in the MATLAB R2015, R2016, and R2017 software language.

Each of the 13 particle size fractions was subjected to several runs. These were combined and averaged to develop reflectance and polarization phase curves associated with each particle size. The number of runs that were averaged for each particle size fraction is shown in Table 1. A single complete run lasted 23 hours. The entire data set used in this study totaled 81 runs.

6. Particle morphology

The Al_2O_3 particulates are supplied in two different particle shapes. The sizes larger than 2.1 µm (WCA) are described by the supplier as 'platelet shaped'; those smaller than 1.5 µm (GB) are described as 'equant' . These morphology differences should be apparent with analysis of particle packing density (void space) as a function of particle size and also in photomicrographs.

6.1. Void space vs. Particle size

The relationship between void space and particle size is shown in Fig. 1. The particle sizes < ~1.5 µm (shown as 'equant' in the figure and designated 'GB') have much more void space than the particles of size > ~ 2.1 µm (Shown as 'Platlet' in Fig. 1 and designated WCA). This is consistent with what is reported by the manufacturer as reported in Nelson et al., 2000, 2002, 2016).

6.2. Atomic force microscopy

One of us (KV) acquired Atomic Force Photomicrographic (AFM) images of the samples. The AFM images were obtained in air in intermittent contact mode using a Quesant Instruments Universal Scanning Probe Microscope, an instrument used extensively in studies on bacteria morphology (see, for example, Vandervoort and Brelles-Mariño, 2014, Vandervoort and Brelles-Mariño, 2013, Vandervoort et al., 2008), housed in the Physics and Astronomy department at the California Polytechnic University at Pomona, CA. Commercial silicon cantilevers from MikroMasch were employed. Images consisted of 500 lines of 500 points per line for a total of 250,000 pixels of data. Al_2O_3 samples were deposited on glass slides, previously cleaned and coated with poly-L-lysine to assure surface adhesion of the sapphire particles to the glass. Typical results are shown in Figs. 2 and 3.

Fig. 2 is an AFM image of three typical particles that are identified by the supplier as having an average diameter, $d = \sim 1.0\,\mu m$ (GB 2000). The three particles also show a range of size about the mean particle size. It is clear that they are equant in character as reported by the manufacturer. Fig. 3 is an AFM image of a particle described by the manufacturer as 22.75 µm diameter. The platlet shape is obvious and consistent with the manufacturer's characterization. The information in Figs. 1–3 should clarify any ambiguity that may have arisen regarding the morphology of these Al_2O_3 materials when they are used as high albedo particulate planetary surface analogues (Nelson et al., 2016).

7. The Helmholtz reciprocity principle

The Reflectance Phase Curves. The reflectance phase curves for three particle size fractions at phase angles $0° < \alpha < 5°$are shown in Fig. 4 (top: 0.1 µm data are plotted as dots, 1.0 µm as squares, and 30.09 µm as diamonds). These particle sizes were selected because they are smaller than, approximately equal to and much larger than the wavelength of the incident radiation. These sizes span the 'forward scattering' and 'backscattering' regimes.

The reflectance phase curves were measured by presenting the sample with alternating states of linearly polarized light and combining the reflected component. For comparison, Fig. 4 (bottom) shows the reflectance phase curves of the same three materials measured in our earlier work in which we placed linear and circular polarizers in the path of the reflected light before it entered the detector.

It is evident from Fig. 4 that the results from the two techniques do not differ within the error. The reflectance phase curves we report are consistent with what would be expected by applying the Helmholtz Reciprocity Principle (HRP).

The Polarization Phase Curves We next measured the response of the same samples to polarized light. The polarization phase curves for Al_2O_3 particles of size 0.1, 0.5 and 1.0 µm are shown in Fig. 5 (top). These measurements were made by presenting the sample with linearly polarized light and measuring the intensity of the reflected component. The linear polarization was calculated by measuring the difference between the intensity measured in the scattering plane compared to that measured perpendicular to the scattering plane divided by the sum of the two. In 2002, we measured the polarization phase curves of these same Al_2O_3 materials using a GPP at the Karazin University in Kharkiv, Ukraine (Shkuratov et al., 2002, see also Ovcharenko et al., 2006). The Karazin University GPP had been previously calibrated to the JPL GPP and the reflectance results from both instruments were consistent when measuring like materials. The Karazin University GPP measures the reflectance and degree of linear polarization at phase angles ranging from 0.2° to 4° at selected spectral bandpasses ($\lambda_{eff} = 0.63$ and $0.45\,\mu m$.). It uses a halogen lamp as a light source. Unpolarized light is presented to the sample, and linear polarizers are placed in the path of the reflected light to measure the polarization. The Karazin University GPP measures polarization identically to the astronomical polarization measurements.

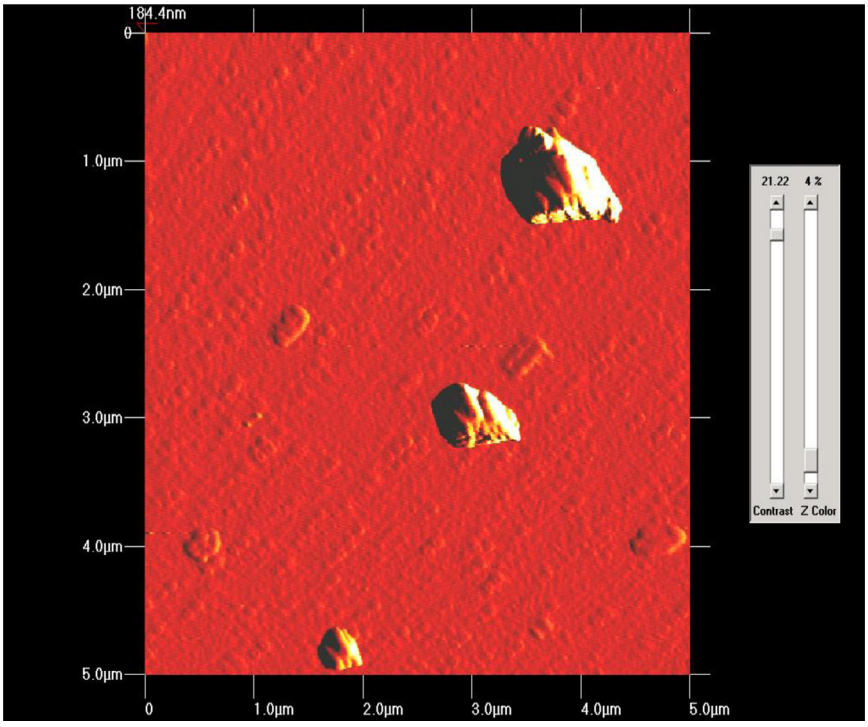

Fig. 2. Atomic Force Photomicrograph of typical Al_2O_3 particles of D = ~ 1.0 µm (GB 2000). The particles are representative of the variation about the mean particle size.

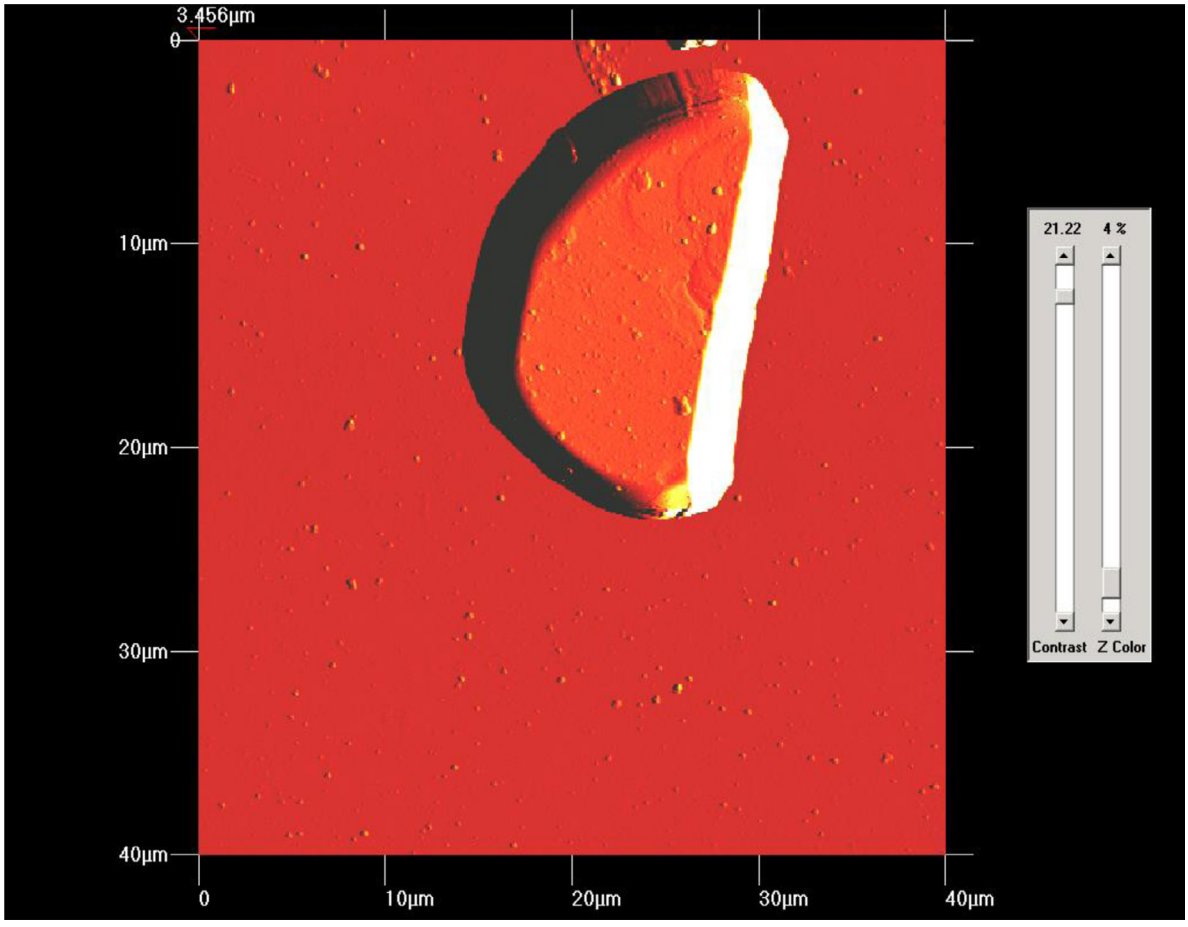

Fig. 3. Atomic Force Photomicrograph of a typical Al_2O_3 particle of D = ~ 22.75 µm. The platlet shape is quite apparent.

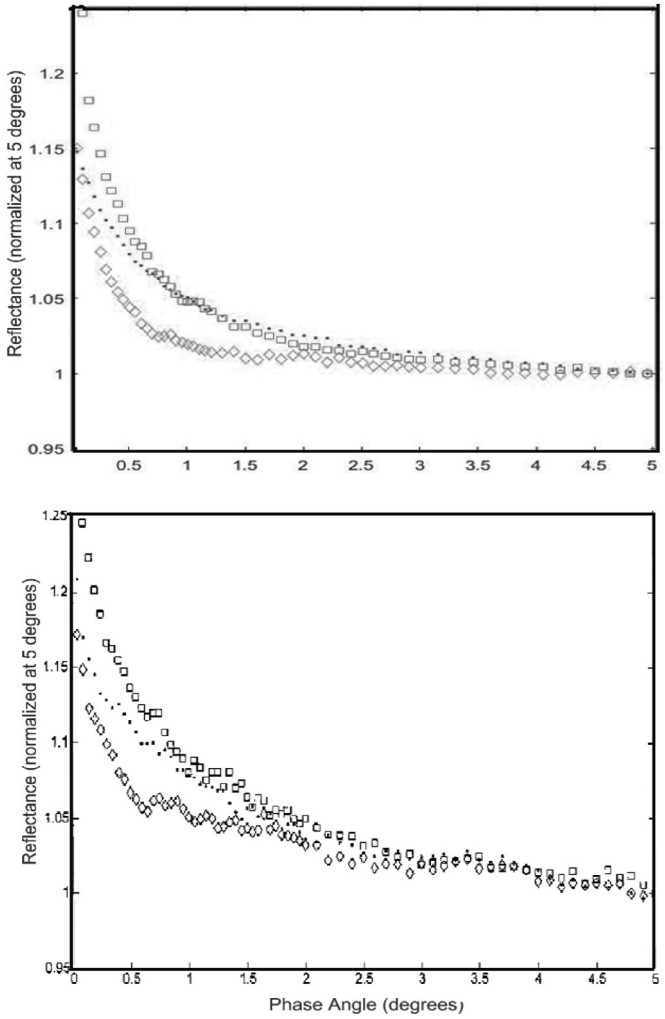

Fig. 4. Top. Reflectance phase curves from this study for three particle sizes of Al_2O_3. Diamonds – 30 μm, Squares – 1.0 μm, Dots- 0.1 μm. Bottom. Same as above except from Nelson et al. (2000). The close agreement of these three reflectance measurements are consistent with the HRP.

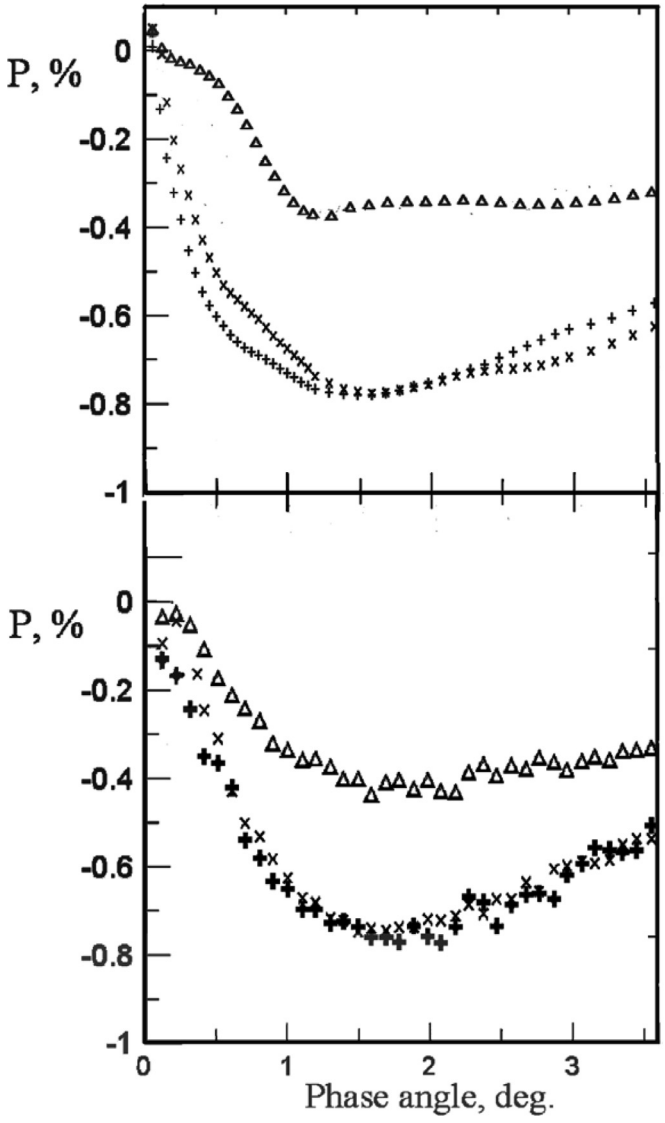

Fig. 5. Top. Polarization phase curves for three particle sizes of Al_2O_3 from the present study in which the samples were presented with polarized light and the intensity of the reflected component was measured. Triangles indicate 1.0 μm, crosses indicate 0.5 μm, and pluses indicate 0.1 μm.
Bottom. Polarization phase curves of the same materials when presented with non-polarized light $\lambda_{eff} = 0.63$) and the polarization of the reflected component was measured (Shkuratov et al., 2002). The absence of a significant difference in these phase curves is consistent with what would be expected based on the Helmholtz reciprocity principle.

The Karazin University GPP results are reproduced in Fig. 5 (bottom). Fig. 5 (top), shows the polarization phase curves from this experiment in which the sample was presented with polarized monochromatic light from a laser light source and the intensity of the reflected component was measured to calculate the polarization. For particle sizes that are larger than, comparable to and smaller than the wavelength of the incident radiation, the polarization phase curves are substantively alike for both instruments. We also confirm the Shkuratov et al. (2002) finding that the polarization phase curves for Al_2O_3 with particle size larger than the wavelength of the incident light exhibit no polarization.

We conclude that the similarity of the reflectance phase curves and the polarization phase curves of the same materials reported here and the previous measurements of the reflectance phase curves reported from the GPP at JPL and the polarization phase curves reported by the GPP at Karazin Institute are consistent with what would be expected assuming the HRP applies over this range of phase angles.

8. Implications for outer solar system research

Our earlier work on these materials spanned a range of phase angle $0° < \alpha < 5°$. We present here the first reflectance and polarization phase curves measured with this GPP for these Al_2O_3 particulates extending to 15°. Laboratory measurements of this type are of great importance for understanding the vast number of small trans-Jovian ASSBs that are only observed from earth or earth orbit at this range of phase angle or smaller where the reflectance and polarization of an hypothesized particulate regolith would be expected to be rapidly changing due to CB effects.

We next present the reflectance and polarization phase curves measured from 0.05–15° for each of our Al_2O_3 samples.

9. The reflectance phase curves

In general, the reflectance phase curves of the thirteen different particle sizes are characterized by (starting from 0.05° and proceeding to increasing phase angle):

1. A very sharp, high reflectance, opposition peak with reflectance rapidly decreasing from $0.05° < \alpha \sim < 3°$ transitioning to,

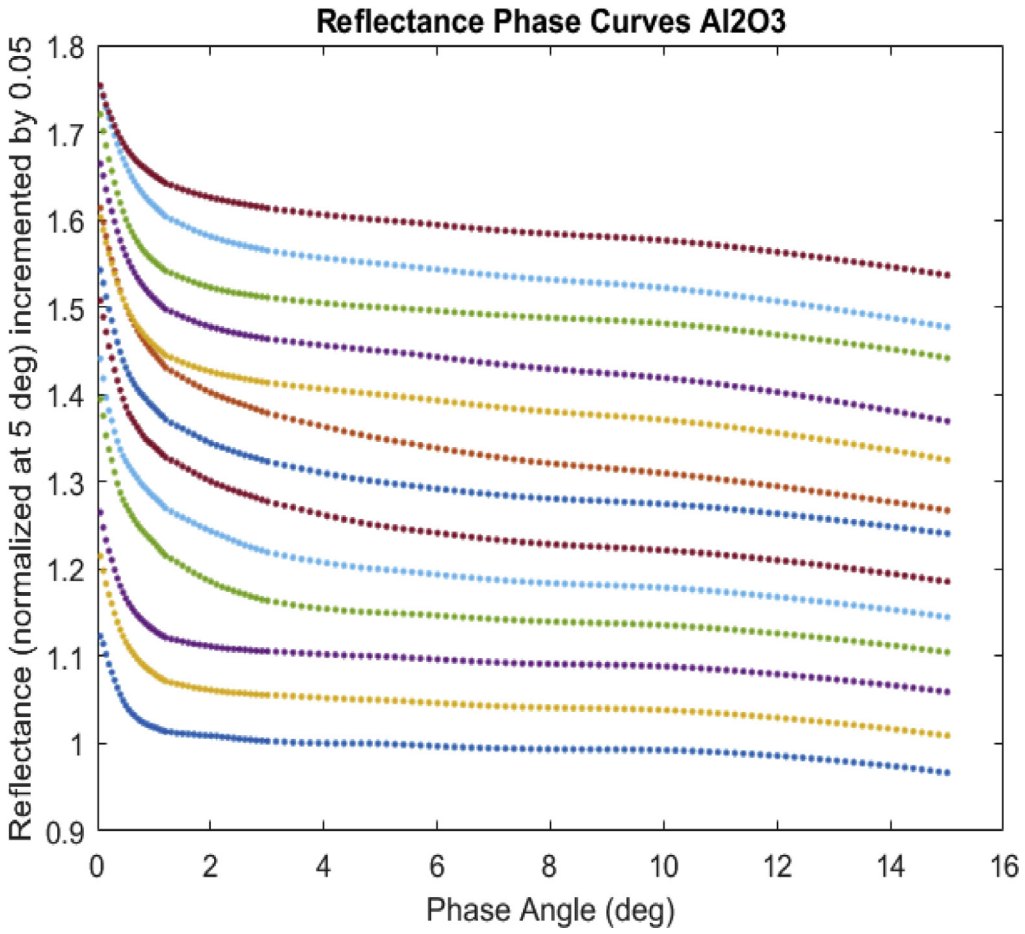

Fig. 6. Reflectance phase curves for the 13 Al_2O_3 samples used in this study normalized at 5°. They are vertically offset by 0.05 for each size. From the bottom to top the phase curves are shown for particle sizes 30.09, 22.75, 12.14, 7.1, 5.75, 4.0, 3.2, 2.1, 1.5, 1.2, 1.0, 0.5, and 0.1 μm respectively. We note the great change in the shape of the phase curve between 1.5 and 2.1 μm. This is most likely a consequence of particle morphology. The particles with $d \leq 1.5$ μm are equant in shape and those with $d >= 2.1$ μm are platlet shaped.

2. A gradual, linearly decreasing reflectance from ~5 – 10°, and
3. A non-linear decrease beyond ~10°.

The reflectance phase curves for the 13 Al_2O_3 particulate samples, normalized at 5°, are shown in Fig. 6. They are displaced vertically by 0.05 for each size. Beginning from the bottom and proceeding upward the phase curves are shown for particle sizes 30.09, 22.75, 12.14, 7.1, 5.75, 4.0, 3.2, 2.1, 1.5, 1.2, 1.0, 0.5, and 0.1 μm respectively.

We note the great difference in the shape of the phase curve between particle sizes $d <= 1.5$ and particle sized $d \geq 2.1$ μm. This is most probably a consequence of particle morphology. The smaller size fractions ($d < \sim 1.5$ μm.) are equant while the larger fractions are platlet in shape. This is also evident from the packing density (Fig. 1 and Table 1) and in the AFM photomicrographs (Figs. 2 and 3). Future theoretical modeling endeavors that purport to infer regolith characteristics based on remote sensing observations are cautioned to carefully consider particle morphology. The Al_2O_3 phase curves reported here compare favorably with earlier work on the same materials (Nelson et al., 2000, Figs 5 and 7, 2002, Figs 4 and 5; Piatek et al., 2004 Fig 2A; Shkuratov et al., 2002 Fig 11; Ovcharenko et al., 2006 Figs 4–6; Shkuratov et al., 2008 Fig. 10).

In our previous work we followed earlier modeling investigations (Mishchenko, 1992; Mishchenko and Dlugach, 1993) and represented the size of the OE in terms of the half width at half maximum (HWHM) of the phase curve for each particle size as a function of the dimensionless size parameter, r/λ. Our experimental results found that the HWHM is largest when the particle size approximates the wavelength of the incident radiation. This is qualitatively in agreement with theoretical modeling results reported by Mishchenko (1992) (see Nelson et al., 2000, Fig 9).

In this study, we use two improved methods to estimate the magnitude of the opposition peak.

First, we calculate the area between the measured phase curve and its extrapolated linear portion from 5 – 10° to estimate the size of the opposition peak. The area is calculated by Simpson's rule using the difference between the measured intensity and the liner extrapolation.

Second, we calculate the size of the opposition peak by subtracting the extrapolated value of the linear portion of the phase curve at 0° from the size of the opposition peak at 0° determined by fitting the expression (hereafter referred as PSIMTSAC1 function)

$$y = \cos(\alpha/2)\left(a \cdot e^{b\alpha} + c \cdot e^{d\alpha}\right) \quad (4)$$

to the data and estimating the peak value, a+c at $\alpha = 0°$. We had attempted this in our earlier work when our range of observations was restricted to $\alpha < 5°$, but the estimating of the linear portion of the phase curve was challenging when making measurements near these small phase angles (Nelson et al., 2000). We used a similar technique in our earlier work where we followed the approach of Akimov (1980), Shkuratov (1983, 1997) and Shkuratov et al. (2011) in using an exponential function to approx-

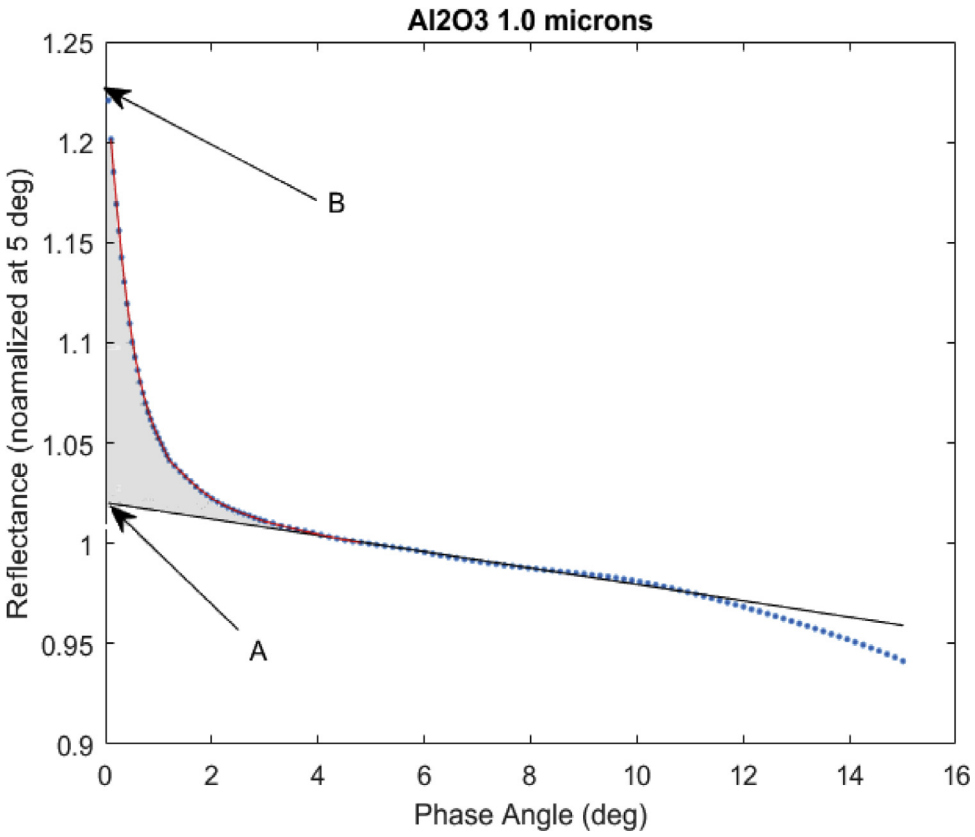

Fig. 7. Phase curve for 1.0 µm Al_2O_3 particles. A straight line is fitted to the data from 5 to 10°. This is extrapolated to 0°. The size of the opposition surge is estimated by two methods. First, we calculated the area (shaded) between the linear region and the phase curve (PSIMTSAC1 function) normalized at 5°. Second, we calculated the difference between the extrapolated linear portion of the curve at 0° (A) and the size of phase curve at 0° (B).

Table 2
Results of fitting PSIMTSAC1 function (Eq. (4)) to the data.

Name	Diameter µm	Area under phase curve 0–5°	Height of opposition Peak	a	b	c	d
GB3000	0.1	69.38	15.15	13.93	−1.73	104.23	−0.0063
GB2500	0.5	88.82	20.71	19.66	−1.66	106.3	−0.0062
GB2000	1.0	90.35	25.66	24.31	−2.16	105.36	−0.0049
GB1500	1.2	92.72	26.01	24.92	−2.001	107.91	−0.0068
GB1200	1.5	96.36	27.02	25.97	−2.05	105.67	−0.00536
WCA 1	2.1	137.67	23.91	22.39	−1.36	103.82	−0.00836
WCA 3	3.2	137.68	26.41	24.67	−1.59	102.6	−0.00669
WCA 5	4.0	139.75	25.36	23.49	−1.49	101.1	−0.00709
WCA 9	5.75	120.25	23.46	21.85	−1.529	98.75	−0.00541
WCA 12	7.1	113.88	22.79	21.62	−1.449	97.15	0.0044
WCA 20	12.14	75.57	20.52	19.55	−1.89	92.83	−0.00423
WCA 30	22.75	44.95	17.56	17.1	−2.54	92.99	−0.0026
WCA 40	30.09	33.40	15.88	15.455	−3.184	91.07	−0.0022

imate the shape of the reflectance phase curve. This heuristic approach has obvious value in applying these results to astronomical observations of ASSBs.

Area under phase curve. The area under the phase curve was calculated for each particle size to estimate the magnitude of the opposition surge. This was done by calculating the area between the curve defined by the PSIMTSAC function (Eq. (1) above) and the linearly extrapolated portion of the phase curve $5° < \alpha < 10°$. It is the shaded area in Fig. 7. Both the maximum of the phase curve and its breadth are indicators of the strength of the opposition surge. The area calculated in this way is an excellent indicator of OE strength because it weights both the height and breadth of the OE peak. The results are tabulated in Table 2.

Extrapolated difference. For each particle size, we fitted a straight line to the phase curve data from 5–10°. A typical fit for the 1.0 µm size is shown in Fig. 7. The straight line was extrapolated to 0°, the size of the opposition surge was calculated by subtracting the value of the linear portion extrapolated to 0° ("A" in Fig 7) from the extrapolated value of the phase curve at 0° ("B" in Fig 7). This indicates only the size of the OE at 0° and attaches no significance to the breadth of the phase curve.

The magnitude of the opposition surge clearly depends both on particle size and, in addition, void space. Table 1 shows that void space increases with decreasing particle size. The OE has a broad maximum for particles whose diameters are around the wavelength of the incident light ($\lambda = 0.635$ µm). This is where CB of the incident photons is maximum. The OE size decreases with decreasing particle size for $d < 1$ µm and decreases with increasing particle size for sizes $d >= 4$ µm. This is evident in Table 2 and Fig. 7.

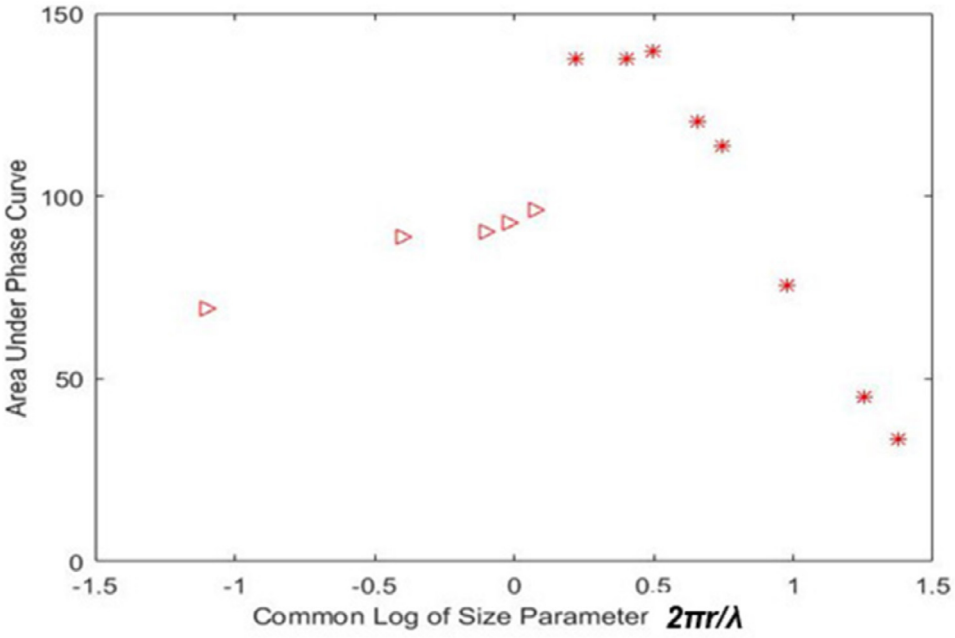

Fig. 8. The area under the phase curve ($\alpha < 5°$) with respect to particle size parameter ($2\pi r/\lambda$) for 13 Al_2O_3 particle sizes. The larger sized particles are platlet shaped and represented as asterisks. The smaller sized particles are equant and represented as triangles. The size of the opposition surge is largest for particles with size parameter 1 (log size parameter = 0).

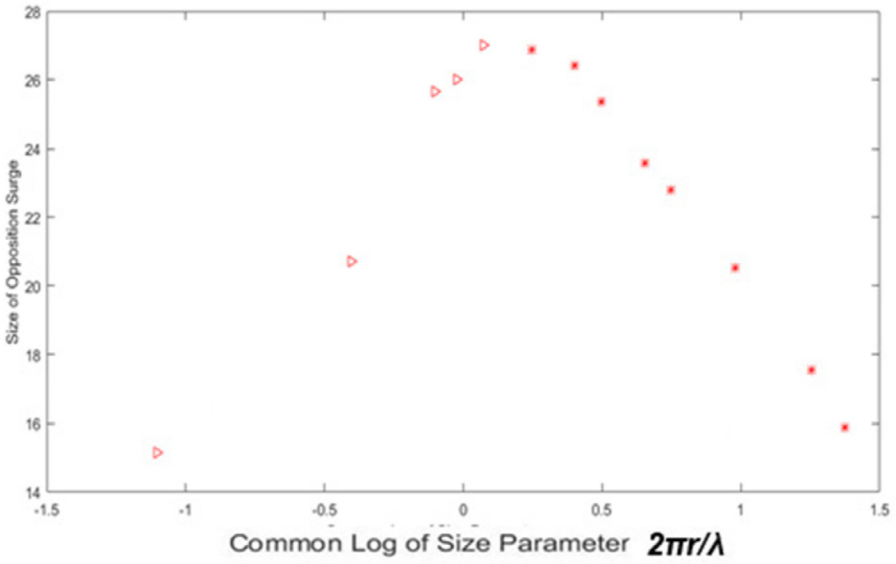

Fig. 9. The size of the opposition surge with respect to particle size parameter ($2\pi r/\lambda$) for the same materials determined by the difference between the extrapolated exponential fit to the data and the extrapolated linear portion of the phase curve, 5–12°.

The relationship between the particle size and the area under the phase curve for $\alpha < 5°$ is shown in Table 2 is shown in Fig. 8. The relationship between the size of the OE determined by the difference between the data extrapolated to 0° from the PSIMTSAC1 function and the liner portion of the phase curve from 5 to 10° extrapolated to 0° is shown in Fig. 9. The size of the opposition effect using either method of determining the magnitude of the OE is greatest for particles with size parameter ~1. The size of the opposition peak and the area under the curve are good indicators of OE strength and correlate with a correlation coefficient of 0.84.

10. The polarization phase curves

We find, consistent with our earlier work (Shkuratov et al., 2002), that these highly reflective Al_2O_3 particulates exhibit a change in linear polarization with phase angle. However, the character of the polarization phase curve differs from what has been previously reported in polarization studies of the Moon, asteroids and highly absorbing material measured in the laboratory (Zellner et al., 1977; Geake et al., 1984. Geake and Dollfus, 1986; Lupishko and Di Martino, 1998.)

The polarization phase curves for size fractions of radius less than or comparable to the wavelength of the incident light are

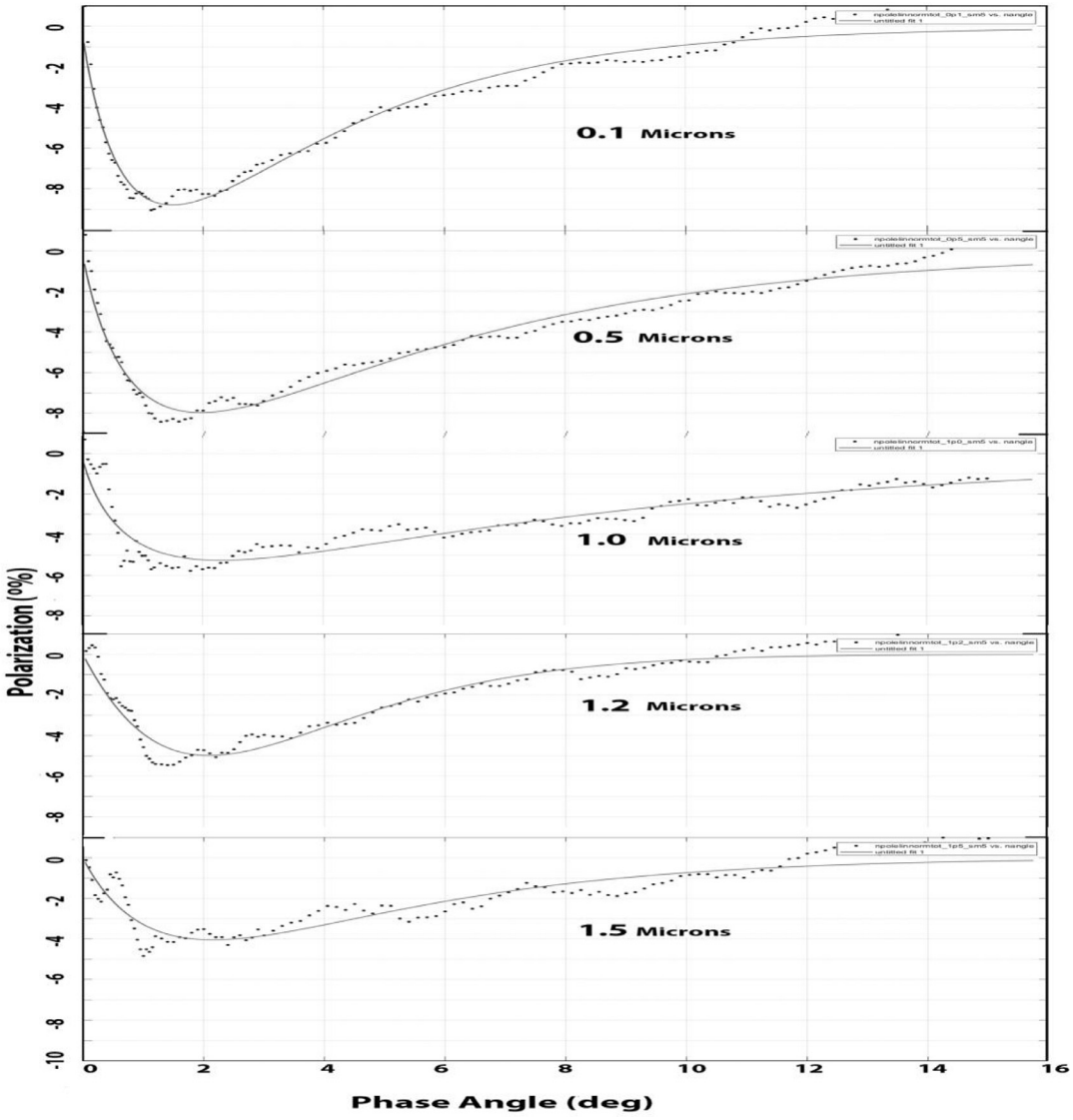

Fig. 10. Polarization Phase Curves of the five smallest Al_2O_3 particle size fractions. The figures are vertically displaced by 1% for each particle size. The solid line is a linear least square fit to the data of PSIMTSAC2 function.

characterized by (starting from $\alpha = 0.05°$ and proceeding to increasing phase angle):

1. A very strong decrease in polarization beginning at $\alpha = 0.05°$ with continued decrease to ~1°, depending on particle size.
2. A polarization minimum between 1° and 2° depending on particle size. The smallest particle sizes exhibit the lowest polarization minimum.
3. After the minimum is reached there is a decrease in negative polarization reaching a crossover point between 12° and 20° (estimated), depending on particle size.

The polarization phase curves for the five smallest particle sizes are shown in Fig. 10. They are displaced vertically by 1% with the smallest particle size at the top of the figure.

The polarization phase curves that we measure can easily be described by a function of the form:

$$P = -\alpha/(1 + a \cdot e^{b\alpha^c}) \quad (5)$$

where 'y' is the polarization, ' α' is the phase angle (in degrees), and 'a', 'b', and 'c' are the best linear least square fit coefficients to each set of data for each particle size.

Table 3
Results of fitting Eq. (5), PSIMTSAC2 to the data.

Particle size (microns)	a	b	c
0.1	43.69	1.005	0.7379
0.5	54.93	0.9533	0.6693
1.0	64.95	1.229	0.5265
1.2	177.2	0.3623	1.168
1.5	169.6	0.5828	0.8757

Eq. (5), PSIMTSAC2, may prove useful to remote sensing observers in efforts to compare these laboratory measurements to astronomical data. Once again, a heuristic approach may prove to be of value to astronomical observers who are assessing the nature of ASSBs, and particularly those who investigate the possible impact hazards of such objects to planet Earth. The fitting was accomplished by using the MATLAB curve fitting functions. The results are shown in Table 3.

Our results are qualitatively consistent with theoretical studies of the angular profile of the polarization opposition effect and are similar to laboratory measurements the polarization of smoked Magnesium Oxide on a glass substrate reported by Lyot nearly a

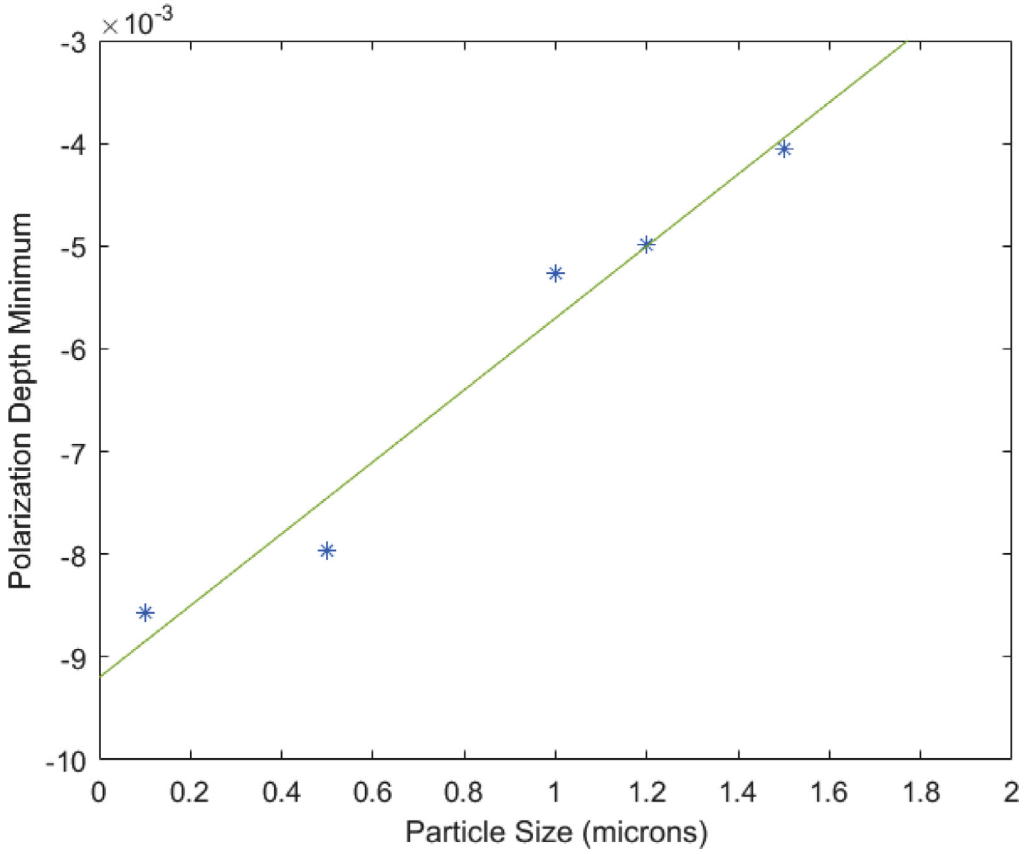

Fig. 11. Relationship between Al_2O_3 particle size vs the depth of the observed polarization minimum for the five smallest size fractions. The line is a least squares best fit line.

century ago. (Mishchenko et al., 2000;2006; Shkuratov et al., 2002 Fig 4).

10.1. Depth of the polarization minimum

We calculated the depth of the polarization minimum for each particle size using the expression PSIMTSAC2 above. The results are plotted with respect to particle size in Fig. 11. The data are fitted with a linear least square fit line defined by:

$$\text{Polarization} = -.0092 + .0035 * \text{d} \quad (6)$$

where d is the particle diameter.

10.2. Location of the polarization minimum

We also find that the phase angle at which the polarization minimum occurs increases with increasing particle size. This is evident in Fig. 12 where the phase angle at which the polarization minimum (based on PSIMTSAC2above) is plotted against particle size. These data are fitted with a linear least squares straight line fit of the form:

$$\text{P} = \mathbf{1.5757} - \mathbf{0.4446} \cdot \alpha \quad (7)$$

11. Discussion

Understanding the reflectance properties of high reflectance particulate ensembles is of great use in understanding those regions of the outer solar system where high albedo objects exist (such as the Galilean satellites Io, Europa and Ganymede) and selected reflective locales on objects such as Ceres and Pluto. These laboratory measurements will be of interest to all observers of ASSBs, particularly those who make observations of trans-Jovian objects from earth or earth orbit. Such observations of trans-Jovian objects are limited to phase angles $\alpha < \sim 10°$. The reflectance change with respect to phase angle provides an important constraint on surface texture after making corrections for rotational changes. The polarization phase curves may also provide an independent constraint on regolith texture.

This reflectance behavior we report might be generalized (with caution) to such locales in the outer solar system where high reflectance is reported, however we caution that this polarization behavior is only observed for Al_2O_3 particles comparable in size or smaller than the wavelength of the incident light which exhibit equant morphology. It might be tempting to assume that the polarization effects we report here can be generalized to all high albedo particulates of small particle size. We have not investigated, as of yet, other particulate materials of different composition and albedo. We suggest that caution be observed when generalizing these results, noting that Shkuratov et al. (2002, Fig 18) report similar polarization behavior in NiCr spheres of large particle size (60 μm) and we note furthermore that these effects have also been reported for low albedo Boron Carbide (B_4C) of large particle size (Ovcharenko et al., 2006). The conjecture that the reflectance behavior reported here might apply to all high albedo particulates of sub-wavelength particle size, while consistent with the theory that underlies CB, remains to be confirmed for a broad range of high reflectance particulates.

We note the striking similarity between the polarization phase curves we report for high porosity assemblages of reflective particulates of Al_2O_3 (a water ice reflectance analog) and the polarization phase curves of the Galilean satellites reported by Rosenbush et al. (1997, Fig. 5, 2015) where water ice has been

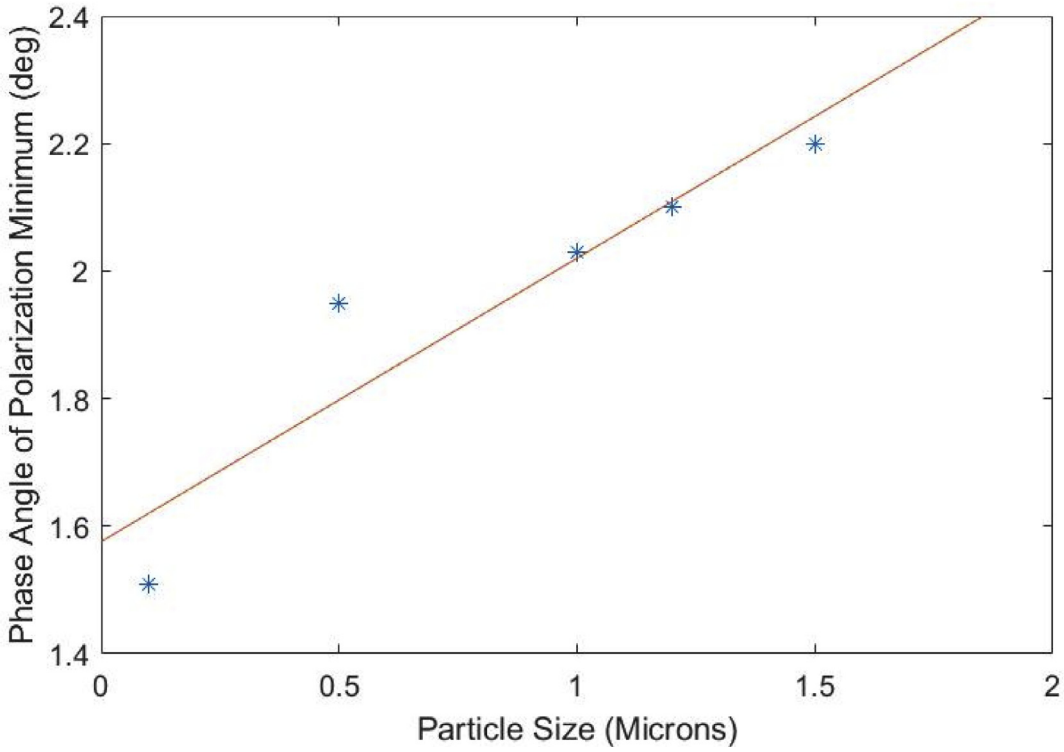

Fig. 12. Relationship between Al_2O_3 particle size and the phase angle of the observed polarization minimum for the five smallest size fractions. The line is a least squares best fit line.

reported based on spectroscopic evidence for a half century (Moroz, 1969). We have not as yet specifically determined whether these properties are caused by small particle size, high void space or both. However, we suggest that this polarization phase curve data from the laboratory, when compared to the telescopic polarization phase curve observations reported by Rosenbush and colleagues, is evidence that Europa may have an extremely porous regolith of fine particles.

The empirical expressions 1 and 2 above can be used simultaneously to refine and constrain the surface models developed by the astronomical observers. This may be the most effective approach to understanding outer solar system objects particularly their potential as hazards to life on Earth.

12. Conclusions

(1) The reflectance and polarization phase curves of highly reflective particulate materials are consistent with the reflectance and polarization properties of selected high albedo solar system objects such as Io, Europa, Ganymede, Saturn's rings and the asteroids 44 Nysa, 64 Angelina (Belskaya et al., 2017 Fig. 4) and could be relevant, if properly interpreted, to understanding high albedo regions such as Sputnik Planum on Pluto (Buratti et al., 2017; Howard et al., 2017), the Occator region on Ceres (De Sanctis, et al. 2017; Schröder et al., 2017), Uranian satellite Umbriel (Sori et al., 2017), Saturn's Moon Enceladus(Scipioni et al., 2017),

(2) The ~0–2° polarization minimum may be associated with) coherent backscattering.

(3) Important features in the polarization phase curve of these particles (such as the slope longward of the polarization minimum correlate strongly with particle size.

(4) Shadow hiding may play a role in lower albedo particles and produce a polarization phase curve by a process different from the process that creates the polarization phase behavior in high albedo particles of small particle size

(5) The science value of future deep space missions to Europa missions would be strongly enhanced if the spacecraft were able to could take polarization phase data, particularly given our laboratory results and the astronomical observations of Vera Rosenbush and colleagues. Obviously, a high porosity regolith would be hazard to spacecraft that landed on Europa's surface, although we note that similar concerns were raised about the lunar regolith before the 1959 landing of the Luna 2 robotic spacecraft and the subsequent human landings by Apollo astronauts.

(6) Laboratory experimentalists with interest in undertaking bidirectional reflectance and polarization measurement might well consider using a GPP design based on the HRP and thereby reduce the number of optical surfaces that the light path must encounter and hence accrue greater signal to noise in their final data products.

13. Afterthought

We note that CB and the HRP are remarkably similar constructs, each positing rays of light traveling the same path but in opposite directions (Wiersma et al., 1995, p 1742). With great respect intended to those who pioneered understanding of CB we suggest that CB might perhaps logically follow from the initial work of Helmholtz himself in 1856.

Acknowledgements

This work was partially supported by NASA's Cassini Saturn Orbiter Visual and Infrared Mapping Spectrometer instrument team (NASA 104479 1.0.12). We gratefully acknowledge Ludmilla Kolokolova, Anny-Chantal Levasseur-Regourd, Padma Yamanda Fisher, William D. Smythe, Frank D. Leader, Roger Clark,

Paul Helfenstein, Karri Muinonen, Yunzhao Wu, Zhang Hao and Dave Blewett. RMN and MB thank Professor Kai Lam of the California State Polytechnic University at Pomona for introducing us to his colleague KV. We thank Professor Charles Newman for loaning us the Mettler-Toledo AE200 Laboratory balance. We thank Evgenij Zubko and an anonymous reviewer for excellent comments made in reviewing this manuscript. RMN deeply appreciates the support of Tony Diaz of Caltech Library Services.

Supplementary materials

Supplementary material associated with this article can be found, in the online version, at doi:10.1016/j.icarus.2017.11.021.

References

Akimov, L.A., 1980. In: Nature of the Opposition Effect, 204. Vestnik Kharkov State University, pp. 3–12.
Akkermanns, E., Wolf, E.P., Maynard, R., 1986. Coherent backscattering of light by disordered media: analysis of the peak line shape. Phys. Rev. Lett. 56, 1471–1474.
Anderson, P.W., 1958. Absence of diffusion in certain random lattices. Phys. Rev. 109, 1492–1505.
Aegerter, C.M., Maret, G., 2009. Coherent backscattering and Anderson localization of light. Optics 52, 1–62.
Barabashev, N.P., 1922. Bestimmung der Erddalbedo und des Reflexionsgesetzes fur die Oberflache der Mondmeere. Theorie der Rillen. Astron. Nachr. 217, 445–452.
Belskaya, I., Cellino, A., Gil-Hutton, R., Muinonen, K., Shkuratov, Y., 2015. Asteroid polarimetry. In: Michel, P., DeMeo, F.E., Bottke, W.F. (Eds.), Asteroids IV. University of Arizona Press, Tucson, pp. 151–163. ISBN 9780816532131.
Belskaya, I.N., Fornasier, S., Tozzi, G.P., Gil-Huttond, R., Cellino, A., Antonyuk, K., Krugly, Y.N., Dovgopol, A.N., Faggi, S., 2017. Refining the asteroid taxonomy by polarimetric observations. Icarus 284, 30–42.
Buratti, B.J., Hofgartner, J.D., Hicks, M.D., Weaver, H.A., Stern, S.A., Momary, T., Mosher, J.A., Beyer, R.A., Verbiscer, A.J., Zangari, A.M., Young, L.A., Lisse, C.M., Singer, K., Cheng, A., Grundy, W., Ennico, K., Olkin, C.B., 2017. Global albedos of Pluto and Charon from LORRI: *new horizons observations*. Icarus 287, 207–217.
Chandrasekhar, S., 1960. Radiative Transfer. General Publishing Company, Toronto, Dover edition, New York ISBN 0-486-60590-6.
De Sanctis, M.C., Raponi, A., Ammannito, E., Ciarniello, M., Toplis, M.J., McSween, H.Y., Castillo-Rogez, J.C., Ehlmann, B.L., Carrozzo, F.G., Marchi, S., Tosi, F., Zambon, F., Capaccioni, F., Capria, M.T., Fonte, S., Formisano, M., Frigeri, A., Giardino, M., Longobardo, A., Magni, G., Palomba, E., McFadden, L.A., Pieters, C.M., Jaumann, R., Schenk, P., Mugnuolo, R., Raymond, C.A., Russell, C.T., 2017. Bright carbonate deposits as evidence of aqueous alteration on (1) Ceres. Nature 536, 54–57.
Deau, E, Flandes, A., Spilker, L.J., Petazzoni, J., 2013. *Re*-analysis of previous laboratory phase curves: 1. Variations of the opposition effect morphology with the textural properties, and an application to planetary surfaces. Icarus 226, 1465–1488.
Dollfus, A., 1996. Saturn's ring: optical reflectance polarimetry. Icarus 124, 237–261.
Etemand, S.R., Thompson, M., Andrwco, M, John, S., MacKintosh, F., 1987. Weak localization of photons: termination of coherent random walks by absorption and confined geometry. Phys. Rev. Lett. 59, 1420–1423.
Galileo, G., 1616. Dialogue concerning the two chief world systems. Stillman Drake Translation, 1981. Modern Library Paperback Edition, 2001, Random House, New York.
Gehrels, T., 1956. Photometric studies of asteroids V. The light curve and phase function of 20 Massalia. Astrophys. J. 123, 331–338.
Geake, J.E., Geake, M., Zellner, B., 1984. Experiments to test theoretical models of the polarization of light by rough surfaces. Mon. Not. R. Astron.Soc. 210, 89–112.
Geake, J.E., Dollfus, A., 1986. Planetary surface texture and albedo from parameter plots of optical polarization data. Mon. Not. R. Astron. Soc. 218, 75–91.
Gunderson, K., Thomas, N., Whitby, J.A., 2006. First measurements with the Physikalische Institut Radiometric Experiment (PHIRE). Planet. Space Sci. 54, 1046–1056.
Hapke, B., 1963. A theoretical photometric function for the lunar surface. J. Geophys. Res. 68, 4571–4586.
Hapke, B., 1966. An improved theoretical lunar photometric model. Astron. J. 71, 333–339.
Hapke, B., 1981. Bidirectional reflectance spectroscopy: 1. Theory. J. Geophys. Res. 86, 3039–3054.
Hapke, B., 1986. Bidirectional reflectance spectroscopy. 4. The extinction coefficient and the opposition effect. Icarus 67, 264–280.
Hapke, B.W., 1990. Coherent backscatter and the radar characteristics of outer solar system planetary satellites. Icarus 88, 407–417.
Hapke, B.W., Blewett, D., 1991. A coherent backscatter model for the unusual radar reflectance of icy satellites. Nature 352, 46–47.
Hapke, B., Nelson, R.M., Smythe, W.D., 1998. The opposition effect of the Moon: coherent backscatter and shadow hiding. Icarus 133, 89–97.
Hapke, B., 1993. Theory of Reflectance and Emittance Spectroscopy, second ed. Cambridge Univ. Press, Cambridge, UK 2012. ISBN-13: 978-0521883498.
Howard, A.D., Moore, J.M., Umurhan, O.M., White, O.L., Anderson, R.S., McKinnon, W.B., Spencer, J.R., Schenk, P.M., Beyer, R.A., Stern, S.A., Ennico, K., Olkin, C.B., Weaver, H.A., Young, L.A.The New Horizons Science Team, 2017. Icarus 287, 287–300.
Irvine, W., 1966. The shadowing effect in diffuse reflection. J. Geophys. Res. 71, 2931.
Kaasalainen, S., Piironen, J., Muinonen, K., Karttunen, H., Peltoniemi, J., 2002. Laboratory experiments on backscattering from regolith samples. Appl. Opt. 41, 4416–4420.
Levasseur-Regourd, A.C., Renard, J.-B., Shkuratov, Y., Hadamcik, E., 2015. Laboratory studies. In: Kolokolova, L., Hough, J., Levasseur-Regourd, A.-C. (Eds.), Polarimetry of Stars and Planetary Systems. Cambridge University Press, United Kingdom, pp. 62–80.
Li, J.-Y., Helfenstein, P., Buratti, B.J., Takir, D., Clark, B., 2015. Asteroid photometry. In: Michel, P., DeMeo, F.E., Bottke, W.F. (Eds.), Asteroids IV. University of Arizona Press, Tucson, pp. 129–150. ISBN 9780816532131.
Lumme and Bowell (1981).
Lupishko, D.F., Di Martino, M., 1998. Physical properties of near-Earth asteroids. Planet. Space Sci. 46, 47–74.
Lyot, B., 1929. Recherches sur la polarisation de la lumiere des planetes et de quelques substances terrestres. Ann. Obs. Meudon. 8, 1–161.
Kuga, Y.L., Ishamaru, A., 1985. Polarization effects of the enhanced retroreflectance from a dense distribution of spherical particles. J. Opt. Soc. Am. A 2, 616–618.
MacKintosh, F., John, S., 1988. Coherent backscattering of light in the presence of time reversal, non-invariant, and parity violating media. Phys. Rev. B 37, 1884–1897.
Minnaert, M., 1941. The reciprocity principle in lunar photometry. Astrophys. J. 93, 403–410.
Mishchenko, M.I., 1992. The angular width of the coherent backscatter opposition effect: an application to icy outer Solar System satellites. Astrophys.Space Sci. 194, 327–333.
Mishchenko, M.I., Luck, J., Nieuwenhuizen, T.M., 2000. Full angular profile of the coherent backscatter opposition effect. J. Opt. Soc. Am. 17, 888–891.
Mishchenko, M.I., Dlugach, J.M., 1993. Can weak localization of photons explain the opposition effect of Saturn's rings? Mon. Not. R. Astron. Soc. 254, 15–18.
Mishchenko, M.I., Rosenbush, V.K., Kiselev, N.N., 2006. Weak localization of electromagnetic waves and opposition phenomena exhibited by high-albedo atmosphereless Solar System objects. Appl. Opt. 45, 4459–4463.
Muinonen, K., 1989. Electromagnetic scattering by two interacting dipoles. In: Proceedings of URSI, International Symposium on Electromagnetic Theory, Stockholm [Reprinted in Muinonen 1990].
Mishchenko, M.I., 2017. Measurement and modeling of electromagnetic scattering by particles and particle groups. In: Kolokolova, L., Hough, J, Levasseur-Regourd, A. (Eds.), Polarimetry of Stars and Planetary Systems. Cambridge University Press, Cambridge UK, pp. 13–32. ISBN-978-1-107-04390-9.
Moroz, V.I., 1969. Physics of Planets 515 Translated from 1967 Russian edition.
Muinonen, K., 1990. Light Scattering By Inhomogeneous media: Backward enhancement and Reversal of Linear Polarization Ph.D. thesis. University of Helsinki.
Nelson, R.M., Hapke, B., Smythe, W.D., Spilker, L.J., 2000. The opposition effect in simulated planetary regoliths. Reflectance and circular polarization ratio change at small phase angle. Icarus 147, 545–558.
Nelson, R.M., Smythe, W.D., Hapke, B.W., Hale, A.S., 2002. Low phase angle studies of the opposition effect: Search for wavelength dependence. Planet. Space Sci. 50, 849–856.
Nelson, R.M., Piatek, J.L., Boryta, M.D., Vandervoort, K., Hapke, B.W., Manatt, K.S., Nebedum, A., Shkuratov, Yu., Psarev, V., Kroner, D.O., Smythe, W.D., 2016. Planetary regolith analogs appropriate for laboratory measurements. In: Proceedings of the Lunar and Planetary Science Conference, p. 1695. Abstract.
Ovcharenko, A.A., Bondarenko, S.Y., Zubko, E.S., Shkuratov, Y.G., Videen, G., Nelson, R.M., Smythe, W.D., 2006. Particle size effect on the opposition spike and negative polarization. J. Quant. Spectrosc. Radiat. Transfer 101, 394–403.
Patterson, G.W, Stickle, A.M., Turner, F.S., Jensen, J.R., Bussey, D.B.J., Spudis, P., Espiritu, R.C., Schulze, R.C., Yocky, D.A., Wahl, D.E., Zimmerman, M., Cahill, J.T.S., Nolan, M., Carter, L., Neish, C.D., Raney, R.K., Thomson, B.J., Kirk, R., Thompson, T.W., Tise, B.L., Erteza, I.A., Jakowatz, C.V., 2017. Bistatic radar observations of the Moon using Mini-RF on LRO and the Arecibo observatory. Icarus 283, 2–19.
Piatek, J.L., Hapke, B.W., Nelson, R.M., Smythe, W.D., Hale, A.S., 2004. Scattering properties of planetary regolith analogs. Icarus 171, 531–545.
Psarev, V., Ovcharenko, A., Yu., Shkuratov, Belskaya, I., Videen, G, 2017. Photometry of surfaces with complicated structure at extremely small phase angles. J. Quant. Spectrosc. Radiat. Transfer 106, 455–463.
Rosenbush, V.R., Avramchuck, V.V., Rosenbush, A.E., Mishchenko, M., 1997. Polarization properties of the Galilean satellites of Jupiter: observations and preliminary analysis. Astrophys. J. 487, 402–414.
Rosenbush, V., Kiselev, N., Afanasiev, V., 2015. Icy Moons of the outer planets. In: Kolokolova, L., Hough, J., Levasseur-Regourd, A-C. (Eds.), Polarimetry of Stars and Planetary Systems. Cambridge University Press, pp. 340–359.
Schröder, S.E, Mottola, S., Carsenty, U., Ciarniello, M., Jaumann, R., Li, J.-Y., Longobardo, A., Palmer, E., Pieters, C., Preusker, F., Raymond, C.A., Russell, C.T., 2017. Resolved spectrophotometric properties of the Ceres surface from dawn framing camera images. Icarus 288, 201–225.
Scipioni, F., Schenk, P., Tosi, F., D'Aversa, E., Clark, R.Combe, J.-P., Dalle Ore, C.M. (Eds.), 2017. Deciphering sub-micron ice particles on Enceladus surface. Icarus 290, 183–200.

Seeliger, H., 1895. Theorie der beliuchtung staubformiger Kosmischen masses insbesondre des Saturnringes. Abhandl. Bayer Akad. Wiss. Math. Nature. 18, 1–72 Kl,II.
Shkuratov, Y., 1983. A model of the opposition effect in the brightness of airless cosmic bodies. Sov. Astron. 27, 581–583.
Shkuratov, Y.G., 1985. On the origin of the opposition effect and negative polarization from atmosphereless bodies. In: Astron. Circular. Sternberg State Astronomical Institute Moscow, pp. 3–6. No. 1400.
Shkuratov, Y.G., 1988. A diffraction mechanism for the formation of the opposition effect of the brightness of surfaces having a complex structure. Kinem. Fiz. Nebes. Tel. 4, 33–39.
Shkuratov, Y.G., 1989. In: A New Mechanism of Formation of Negative Polarization of Light Scattered By the Solid Surfaces of Cosmic Bodies, 23. Astronomical Observatory of Kharkov State University, pp. 176–180. Translated from Astron. Vestnik.
Shkuratov, Y.G., 1997. A mechanism of the opposition brightness effect of comets and zodiacal-light dust. Sol. Syst. Res. 31, 239–241.
Shkuratov, Y.G., Melkumova, L.Y., 1991. Diffraction model of the negative polarization of light scattered by atmosphereless celestial bodies. In: Lunar and Planet. Sci. Conf. XXII. LPI Houston, pp. 1243–1244. Abstract.
Shkuratov, Y.G., Muinonen, K., 1992. Interpreting asteroid photometry and polarimetry using a model of shadowing and coherent backscattering. In: Harris, A.W., Bowell, E. (Eds.), Asteroids, Comets, Meteors. Lunar and Planetary Institute, Houston, pp. 549–552.
Shkuratov, Y.G., Muinonen, K., Bowell, E., Lumme, K., Peltoniemi, J., Kreslavsky, M.A., Stankevich, D.G., Tishkovetz, V.P., Opanasenko, N.V., Melkumova, L.Y., 1994. A critical review of theoretical models for the negative polarization of light scattered by atmosphereless solar system bodies. Earth Moon Planets 65, 201–246.
Shkuratov, Y., Ovcharenko, A., Zubko, E., Miloslavskaya, O., Muinonen, K., Piironen, J., Nelson, R., Smythe, W., Rosenbush, V., Helfenstein, P., 2002. The opposition effect and negative polarization of structural analogs for planetary regoliths. Icarus 159, 396–416 2002.
Shkuratov, Y.G., Stankevich, D.G., Petrov, D.V., Pinet, P.C., Cord, A.M., Daydou, Y.H., 2005. Interpreting photometry of regolith-like surfaces with different topographies: shadowing and multiple scatter. Icarus 173, 3–15.
Shkuratov, Y.G., Grynko, Y., 2005. Light scattering by media composed of semitransparent particles of different shapes in ray optics approximation: consequences for spectroscopy, photometry, and polarimetry of planetary regoliths. Icarus 173, 16–28.
Shkuratov, Y., Bondarenko, S., Ovchagenko, A., Pieters, C., Hiroi, T., Volten, H., Munoz, O., Videen, G., 2006. Comparative studies of the reflectance and degree of linear polarization of particulate surfaces and independently scattering particles. J. Quant. Spectrosc Radiat. Trans. 100, 340–358.
Shkuratov, Y., Bondarenko, S., Kaydash, V., Videen, G., Munoz, O., Volten, H., 2007. Photometry and polarimetry of particulate surfaces and aerosol particles over a wide range of phase angles. J. Quant. Spectrosc. Radiat. Trans. 106, 487–508.
Shkuratov, Y., Ovcharenko, A.A., Psarev, V., Bondarenko, S.Y., 2008. Laboratory measurements of the reflected light intensity and polarization for selected particulate sufaces. In: Kokhansovsky, A.A. (Ed.). Light Scattering Reviews, 3 Chapter 10. Springer, Berlin ISBN 978-3-540-48305-2.
Shkuratov, Y., Kaydash, V., Korokhin, V., Velikodsky, Y., Opanasenko, N., Videen, G., 2011. Optical measurements of the Moon as a tool to study its surface. Planet. Space Sci. 59, 1326–1371.
Shkuratov, Y., Opanasenko, N., Korokhin, V., Videen, G., 2015. The Moon. In: Kolokolova, L., Hough, J., Levasseur-Regourd, A.-C. (Eds.), Polarimetry of Stars and Planetary Systems. Cambridge University Press, United Kingdom, pp. 303–319.
Sori, M.M., Bapst, J., Bramson, A.M., Byrne, S., Landis, M.E., 2017. A Wunda-full world? Carbon dioxide ice deposits on Umbriel and other Uranian moons. Icarus 290, 1–13.
Stankevich, D., Shkuratov, Y., 2004. Monte Carlo ray-tracing simulation of light scattering in particulate media with optically contrast structure. J. Quant. Spectrosc. Radiat. Transf. 87, 289–296.
Stankevich, D., Istomina, L., Shkuratov, Y., Videen, G., 2007a. The coherent backscattering effects in a random medium as calculated using a ray tracing technique for large non-transparent spheres. J. Quant. Spectrosc. Radiat. Transfer 106, 509–519.
Stankevich, D., Istomina, L., Shkuratov, Y., Videen, G., 2007b. Electromagnetic phase differences in the coherent backscattering enhancement mechanism for random media consisting of large non-transparent spheres. Appl. Opt. 46, 1562–1567.
Steven, M.J., Cwillch, G., 1986. Raliegh scattering and weak localization: effects of polarization. Phys. Rev. B 34, 7564–7572.
Teller, E., Wood, L., Hyde, R., 1997. Global Warming and Ice Ages UCRL-JC-128715.
Umov, N., 1905. Chromatische depolarisation durch Lichtzerstreuung. Phys. Zeit. 6, 674–676.
van de Hulst, H.C., 1957. Light Scattering by Small Particles. General Publishing Company Toronto, New York Dover edition 1981. ISBN 0-486-64228-3.
Van Albada, M.P., Lagendijk, A., 1985. Observation of weak localization of light in a random medium. Phys. Rev. Let. 55, 2692–2695.
Vandervoort, K.G., Brelles-Mariño, G., 2014. Plasma-mediated inactivation of pseudomonas aeruginosa biofilms grown on borosilicate surfaces under continuous culture system. Plos One 9, 1–8.
Vandervoort, K.G., Brelles-Mariño, G., 2013. Cal poly pomona NUE project: implementing microscale and nanoscale investigations throughout the undergraduate curriculum. J. Nano Educ. 5, 51–60.
Vandervoort, K.G., Abramzon, N., Brelles-Mariño, G., 2008. Plasma interactions with bacterial biofilms as visualized through atomic force microscopy. IEEE Trans. Plasma Sci. 36, 1296–1297.
Weidner, V.R., Hsia, J.J., 1981. Reflection properties of pressed polytetrafluoroethylene powder. J. Opt. Soc. Am. 71, 856–861.
Wiersma, D.S., van Albada, M.P., Lagendijk, A., 1995. Coherent backscattering of light from amplifying random media. Phys. Rev. Lett. 75, 1739–1742.
Wolf, P.-E., Maret, G., 1985. Weak localization and coherent backscattering of photons in disordered media. Phys. Rev. Lett. 55, 2696–2699.
Zellner, B., Leake, M., Lebertre, T., Duseaux, M., Dollfus, A., 1977. The asteroid albedo scale. I. Laboratory polarimetry of meteorites. In: Proc. Lunar Sci. Conf. 8th, p. 1110.